

Surgical Agent Orchestration Platform for Voice-directed Patient Data Interaction

Hyeryun Park^{1,4}, Byung Mo Gu^{1,2}, Jun Hee Lee^{1,2}, Byeong Hyeon Choi^{1,2,3},
Sekeun Kim⁴, Hyun Koo Kim^{1,2,3*}, Kyungsang Kim^{4*}

¹Image Guided Precision Cancer Surgery Institute, College of Medicine, Korea University, Seoul, Republic of Korea.

²Department of Thoracic and Cardiovascular Surgery, Korea University Guro Hospital, College of Medicine, Korea University, Seoul, Republic of Korea.

³Department of Biomedical Sciences, College of Medicine, Korea University, Seoul, Republic of Korea.

⁴Department of Radiology, Massachusetts General Hospital and Harvard Medical School, Boston, Massachusetts, USA.

*Co-correspondence: kimhyunkoo@korea.ac.kr; kkim24@mgb.org;

Abstract

In da Vinci robotic surgery, surgeons' hands and eyes are fully engaged in the procedure, making it difficult to access and manipulate multimodal patient data without interruption. We propose a voice-directed Surgical Agent Orchestrator Platform (SAOP) built on a hierarchical multi-agent framework, consisting of an orchestration agent and three task-specific agents driven by Large Language Models (LLMs). These LLM-based agents autonomously plan, refine, validate, and reason to map voice commands into specific tasks such as retrieving clinical information, manipulating CT scans, or navigating 3D anatomical models on the surgical video. We also introduce a Multi-level Orchestration Evaluation Metric (MOEM) to comprehensively assess the performance and robustness from command-level and category-level perspectives. The SAOP achieves high accuracy and success rates across 240 voice commands, while LLM-based agents improve robustness against speech recognition errors and diverse or ambiguous free-form commands, demonstrating strong potential to support minimally invasive da Vinci robotic surgery.

1 Introduction

In robot-assisted surgery using the da Vinci surgical system, the primary surgeon must concentrate with their hands and eyes fully engaged in the surgical procedure. However, accessing and manipulating patient data during the procedure requires the surgeon to shift attention away from the surgeon console and use another monitor or auxiliary interfaces such as TilePro (Intuitive Surgical). These interruptions during surgery become more significant when surgeons need to check various types of multimodal data, including clinical information, CT images, MRI images, and 3D models. Such demands underscore the need for a dynamic interaction system to support minimally invasive robotic surgery. Early interaction studies on voice-controlled robotic surgery mainly focused on camera and equipment manipulation using systems such as AESOP [1–4], the HERMES operating room control center [5], and PARAMIS [6]. These systems were shown to reduce operation time and minimize the need for a second assistant [4], while improving surgical efficiency and reducing communication burden among the operating room staff [5].

Subsequent research extended the scope to a broader range of tasks, including image retrieval and 3D distance measurement [7], real-time camera tracking and zoom control [8, 9], and tissue manipulation through robotic assistant arms [10]. Recent studies have progressed toward interpreting natural language commands utilizing Large Language Models (LLMs). A ChatGPT-integrated system interpreted free-form user speech, and matched it to the most relevant predefined command [11]. In addition, LLM-integrated mixed reality systems enable natural language-driven robot operation [12] and real-time surgery assessment and procedure guidance [13].

LLMs exhibit advanced capabilities for understanding and generating natural language and such models include GPT-4 [14], PaLM [15], LLaMA [16–19], and Gemma [20–22]. These models can interpret natural instructions and perform multi-step problem solving through advanced prompting and reasoning techniques, including Chain-of-Thought (CoT) [23], Self-Consistency CoT [24], Tree-of-Thought [25], and Graph-of-Thought [26]. These advancements in reasoning have transformed LLMs from language generators into autonomous agents that can perceive their environment, plan to achieve specific goals, and act accordingly [27–29]. Various frameworks such as ReAct [30], AutoGPT, BabyAGI, AutoGen [31], and CAMEL [32] have been proposed to integrate reasoning and action. Recent research further applies reinforcement learning to help LLMs learn from past reasoning failures and optimize their decision-making [33]. These diverse reasoning and interaction methods have become the driving force of LLM-based autonomous agents capable of planning, tool use, and collaborative problem solving.

The LLM-based agent typically consists of five key modules: a profile module that defines objectives and constraints, a memory module that stores past states and actions, a reasoning and planning module that formulates strategies for goal achievement, an action module that executes tasks via models, tools, or APIs, and a feedback module that evaluates outcomes and refines future behavior [34]. These agents can operate as a single-agent system using one LLM or as a multi-agent system (MAS) that utilizes specialized agents for distinct tasks, offering advantages in scalability, efficiency, and coordinated workflows [35, 36]. The coordination in MAS is enabled by LLM-based orchestration, where an LLM functions as the cognitive core of the system to manage interactions among agents, planning execution sequences, interpreting intermediate results, and controlling the overall workflow [37–41]. Such MAS systems can be classified as centralized, decentralized, or hierarchical, exhibiting cooperative, competitive, or negotiated behaviors [36, 37]. To implement such orchestration in practice, various agent frameworks have been developed, including LangGraph [42], AutoGen [31], LlamaIndex [43], CrewAI, and AgentKit.

In this work, we highlight the importance of effective interaction between surgeons and surgical tools during procedures, with voice interaction offering a promising approach. Based on this motivation, we modularize key tool functionalities into specialized agents and coordinate them through an orchestrator. Specifically, we introduce a voice-directed Surgical Agent Orchestrator Platform (SAOP) that interprets free-form voice commands to enable context-aware, multimodal data interaction directly on surgical videos. To our knowledge, this is the first hierarchical multi-agent framework, consisting of workflow orchestrator agent and multiple task-specific agents as demonstrated in Fig.1.

In contrast to previous research that relied on predefined commands or a single LLM for direct mapping between voice commands and functions, our SAOP autonomously plans and executes functions through intermediate steps, providing more flexible and robust mapping for complex voice commands. The workflow orchestrator agent uses an LLM to perform probabilistic decision-making across workflow functions and task-specific agent functions, predicting which function to execute next. Within workflow functions, real-time audio function obtains voice input, Speech-to-Text (STT) function transcribes it, correction and validation function uses LLM to revise the command and determine its validity, and the command reasoning function leverages LLM to determine the appropriate task agent. The Information Retrieval (IR) agent retrieves relevant clinical information, the Image Viewer (IV) agent slides through axial, coronal, and sagittal planes of CT scans with zoom operations, and the Anatomy Rendering (AR) agent manages 3D anatomical models through structure selection and view selection, rotation, and zoom control. Each task-specific agent includes an action determination function that leverages an LLM to infer the appropriate action and its parameters. The SAOP also utilizes a memory state that stores previous commands, agents, and various parameters for continuous task execution and adaptive responses to ambiguous commands. To evaluate the SAOP performance, we construct a command dataset consisting of 240 user commands, each annotated with three hierarchical categories: command structure (single or composite), command type (explicit, implicit, or natural language question), and command expression (baseline, abbreviation, or paraphrase).

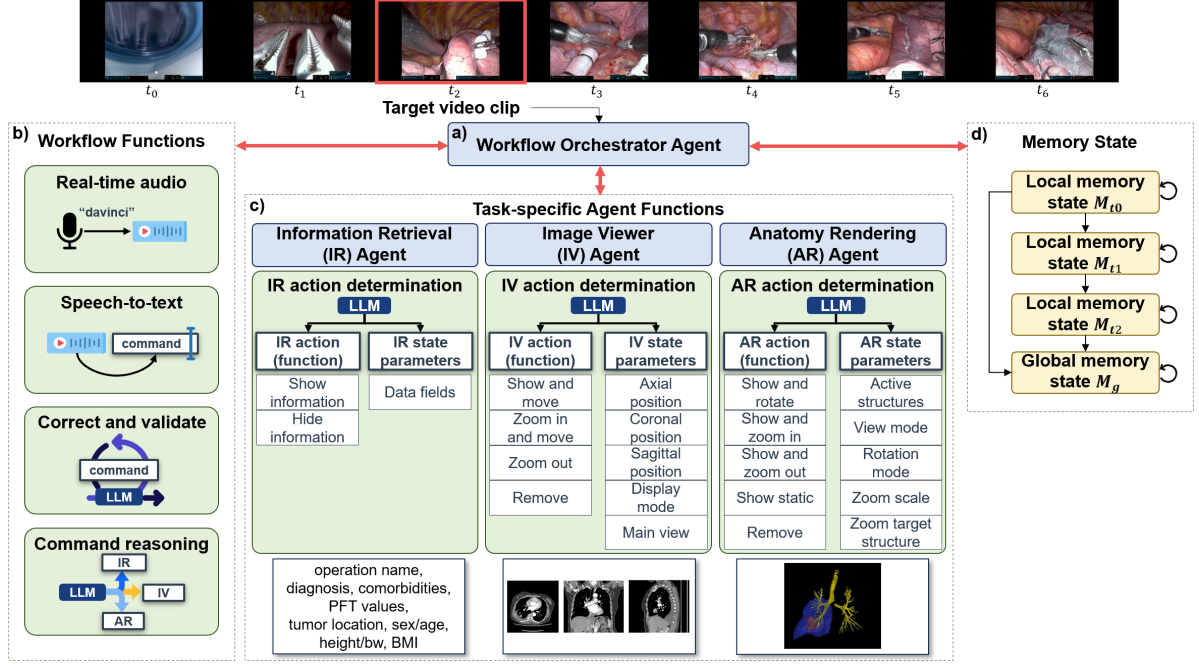


Fig. 1 Overall framework of the voice-directed Surgical Agent Orchestrator Platform (SAOP). **a** Workflow Orchestrator Agent that autonomously plans the order of function execution. **b** Workflow functions that capture, transcribe, correct, and interpret voice commands. **c** Task-specific agent functions that overlay and manipulate patient data on the target video clip. **d** Memory state with local memory states for each video clip and a global memory state for shared contextual understanding across frames.

We further introduce a Multi-level Orchestration Evaluation Metric (MOEM) to assess stage-level accuracy and workflow-level success rates comprehensively. Experimental results demonstrate that voice-directed SAOP achieves high accuracy and success rates, and shows robust flexibility in handling linguistic variability, speech recognition errors, and ambiguous commands through LLM-based command correction and reasoning. Moreover, the design of SAOP establishes it as a flexible platform that supports the integration of new functions and tasks, ensuring scalability and plug-and-play compatibility.

2 Results

2.1 Evaluation metrics

For each command, we evaluate the outcome of every SAOP workflow stage using a binary classification scheme, where 1 denotes a correct result and 0 denotes an incorrect one. Table 1 provides some evaluation results, and Supplementary Data 1 presents the full results for all commands. STT checks whether the command is accurately transcribed, command correction (CC) evaluates the correctness of the revised command, and command reasoning (CR) determines whether the LLM assigns the command to the appropriate agent. Agent function (AF) and agent parameters (AP) are outputs of the action determination (AD) function, and AD is correct only if both AF and AP are accurate. Orchestration flow (OF) evaluates whether the workflow proceeds in the correct order, while invalid cycle (IC) counts how many times the workflow enters an invalid loop. Finally, we propose a Multi-level Orchestration Evaluation Metric (MOEM) to comprehensively assess the performance and robustness of our voice-directed SAOP from two perspectives: (1) command-level orchestration evaluation and (2) command-category evaluation.

The command-level orchestration evaluation measures two aspects of performance: the stage-level accuracy that reflects how accurately each command progresses through individual workflow stages, and the workflow-level success rate (SR) that quantifies the overall success throughout the entire workflow.

The stage-level accuracy is the mean of binary outcomes across all commands for each stage:

$$\text{Accuracy}_{stage} = \frac{1}{N} \sum_{i=1}^N o_{i,stage}, \quad o_{i,stage} \in \{0, 1\} \quad (1)$$

where N denotes the total number of commands, i indicates the command index, and $o_{i,stage}$ represents the binary result of the i -th command at a specific stage. The workflow-level success rate (SR) evaluates each command under three conditions: strict, single-pass, and multi-pass (Fig. 2). For every command i , a binary label $o_{i,condition} \in \{0, 1\}$ indicates whether the command satisfies the corresponding success condition, and the $SR_{condition}$ is the mean of these binary labels over all N commands:

$$SR_{condition} = \frac{1}{N} \sum_{i=1}^N o_{i,condition}, \quad condition \in \{\text{strict, single-pass, multi-pass}\} \quad (2)$$

The command-category evaluation investigates how linguistic and structural variations among commands influence orchestration performance. We compute the category-wise $SR_{multi-pass}$ to identify which categories are more prone to errors or less robust in reasoning. For each category c , the $SR_{multi-pass}$ is the average of the binary outcomes:

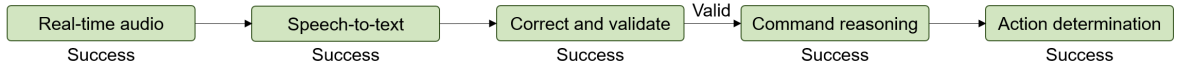
$$SR_{multi-pass}(c) = \frac{1}{N_c} \sum_{i \in c} o_{i,multi-pass} \quad (3)$$

where N_c denotes the number of commands belonging to category c . We also compute the cross-category $SR_{multi-pass}$ along the hierarchy of structure, type, and expression to explore how different linguistic and structural factors jointly affect orchestration performance. For each pair of adjacent levels (structure-type and type-expression), the $SR_{multi-pass}$ is computed for every category pair (c_1, c_2) as:

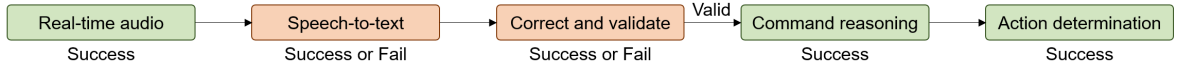
$$SR_{multi-pass}(c_1, c_2) = \frac{1}{N_{c_1, c_2}} \sum_{i \in (c_1, c_2)} o_{i,multi-pass} \quad (4)$$

where N_{c_1, c_2} is the number of commands classified under the pair of categories (c_1, c_2) .

a) Strict success condition



b) Single-pass success condition



c) Multi-pass success condition

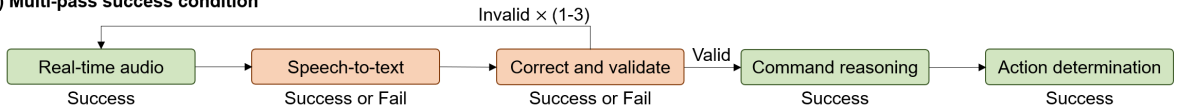


Fig. 2 Success conditions for workflow-level SR. Green boxes represent successful stages, whereas red boxes denote stages that may either succeed or fail. **a** In the strict condition, the command is successful only if all workflow stages succeed without entering any invalid loops. **b** In the single-pass condition, the command is also successful when any intermediate failures are resolved in later stages, leading to a correct final outcome in a single attempt without any invalid loop. **c** In the multi-pass condition, the command is successful when it achieves a correct final outcome after multiple attempts, allowing up to three invalid loops.

2.2 Command-level orchestration evaluation

2.2.1 Stage-level accuracy

The voice-directed SAOP demonstrates strong error recovery capability from STT stage failures, maintaining high accuracy across subsequent stages (Fig. 3a). Investigating each stage in detail, the real-time audio stage accuracy represents the performance of the wake-word detection model for the keyword “davinci”, which correctly recognized 266 out of 300 attempts (88.6%). The remaining 34 attempts were misrecognized, corresponding to a false rejection rate of 11.3%, mainly due to the model misinterpreting “davinci” such as “Dabinci”, “David”, “Benchi”, “dubbing”, or “I’ve been”. For 266 successful cases, the latency between speech detection and the final “davinci” recognition averaged 1.97 seconds, allowing smooth real-time interaction. Stage accuracies from STT to AD are computed using the metric defined in the Eq. (1). Although the STT shows lower accuracy due to transcription errors in the raw audio, most errors are corrected in the CC stage. The CR stage maintains high accuracy in selecting the appropriate agent, and only a slight decrease appears in the AD stage due to occasional mispredictions of the agent function or parameters. Finally, the OF achieves 100% accuracy, confirming that all workflow stages execute in the correct order.

The stage-level accuracies across the three task-specific agents exhibit similar trends (Fig. 3b). Among them, the STT stage shows the greatest variation with the IV agent exhibiting the lowest accuracy due to frequent misrecognition of “CT” as “city”. Nevertheless, most of these recognition errors are corrected during the CC stage, the subsequent CR stage also maintains consistently high performance across all agents, and the AD stage shows a slight decrease. Later stages generally show lower accuracy than the CC stage, reflecting the natural accumulation of prediction errors when performing tasks step-by-step with an LLM. Interestingly, the IR agent fully compensates for imperfectly corrected commands during the CR stage. For example, when the STT transcribes “age info” as “Age in full”, the CC stage refines it to “Age information in full”, allowing the CR stage to infer the intent as a request for the age column only. Overall, these results demonstrate that our platform exhibits strong robustness, effectively mitigating early-stage errors and ensuring accurate agent execution.

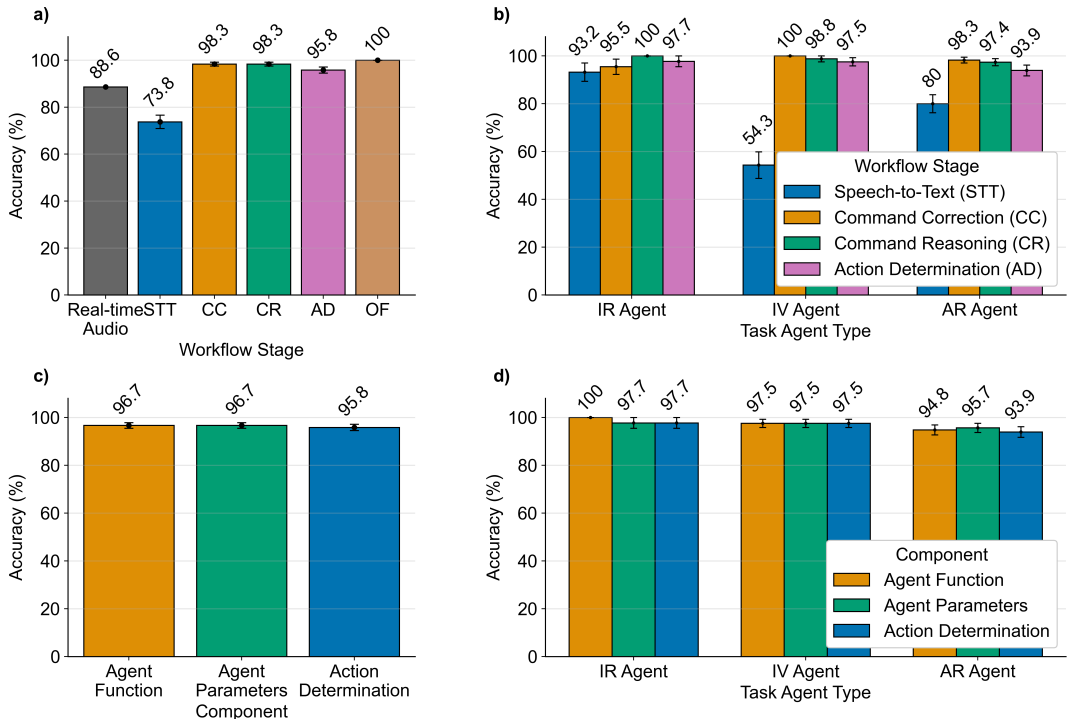


Fig. 3 Overall and task agent-specific stage-level accuracy. a Overall stage-level accuracy. b Stage-level accuracy by task agent type. c Overall accuracy of action determination components d Action determination component accuracy by task agent type. Error bars in all plots indicate 95% confidence intervals.

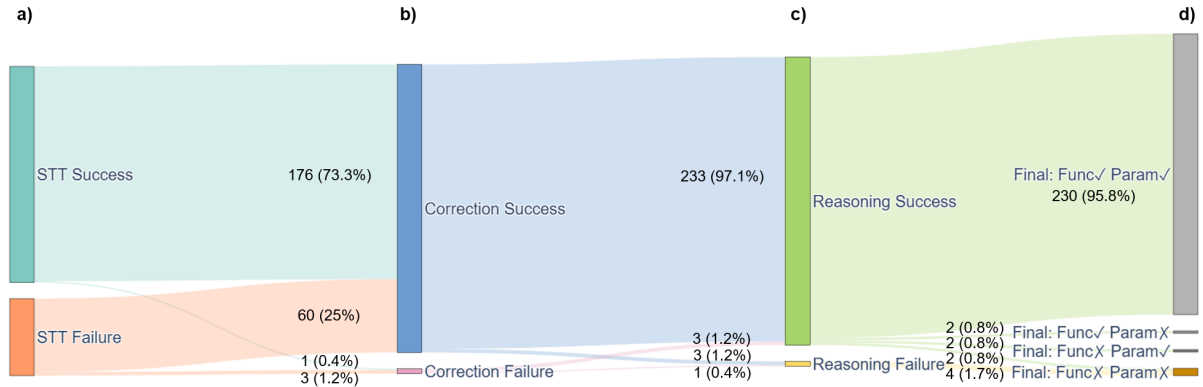


Fig. 4 Command processing flow through workflow stages. A sankey diagram illustrating how commands traverse the LLM-driven stages from a) STT, b) CC, c) CR, and d) AD, visualizing recovery and failure paths.

In the AD stage, each task-specific agent determines the action uniquely mapped to an agent function, and its parameters specifying how the action should be executed. Our SAOP achieves consistently high accuracy for the function and parameters, and because the mispredictions in the two components do not overlap, the combined AD accuracy is slightly lower (Fig. 3c). The accuracies across the three task agents exhibit similar trends, where the integrated AD accuracy is comparable to or slightly lower than the accuracies of function and parameter predictions (Fig. 3d). A slight decrease in accuracy from the IR to IV and AR agents is likely due to the increased variability and complexity of the manipulation commands in the latter tasks. Nevertheless, the differences remain marginal, indicating that the LLM effectively generalizes its reasoning capabilities across heterogeneous task agents.

We further analyze failure and recovery cases along the workflow from STT to AD, identifying bottlenecks and opportunities for improving robustness (Fig. 4; Supplementary Note 1). Most STT errors occur when the model confuses medical or anatomical terminology with phonetically similar non-medical words, such as recognizing “CT” as “city”, “coronal” as “corona”, “lung” as “long”, “lobe” as “loop”, and “trachea” as “track here” (Fig. 4a). Minor lexical errors also occur, such as recognizing “to” as “2”, “right” as “write”, “zoom” as “June”, “info” as “in full”, and “add” as “at”. Although most STT errors are resolved at the CC stage, a few remain, often converting domain-specific terms into non-medical words or nouns into adjective forms (Fig. 4b). In the CR stage, failures occur when the command remains invalid after correction, whereas recovery cases involve minor failure cases in the CC stage that do not affect agent selection (Fig. 4c). In the AD stage, most failures arise from composite commands requiring multiple actions (Fig. 4d). Some failures involve selecting the correct function but incorrect parameters, and others show the opposite pattern. These results highlight the need to support multi-step sequential agent actions and refine prompts to handle specific failure cases.

2.2.2 Workflow-level success rate

The workflow-level SR is evaluated under three conditions as defined in Eq. (2), and the overall performance improves progressively from strict to single-pass to multi-pass conditions (Fig. 5). The SR_{strict} remains at 65.8%, primarily limited by transcription errors in the STT stage. In contrast, the $SR_{single-pass}$ increases to 89.2% as the LLM effectively compensates for early-stage recognition errors through correction and reasoning without entering any invalid loop. The $SR_{multi-pass}$ reaches 95.8%, demonstrating that the workflow orchestrator agent autonomously returns to the real-time audio stage for invalid commands, allowing the user to restate the command more clearly and ultimately achieve successful execution. The task-specific agents exhibit consistent trends, where the SR_{strict} is the lowest across all agents, and performance progressively improves under single-pass and multi-pass conditions (Fig. 5b). Among the agents, the IV agent exhibits the largest gap between strict and single-pass condition due to frequent STT errors, whereas the IR agent shows the smallest gap. As task complexity and command diversity increase from IR to IV and AR, both $SR_{single-pass}$ and $SR_{multi-pass}$ gradually decrease. Overall, these results indicate that performance varies depending on agent characteristics but consistently highlight the robustness and adaptability of our platform.

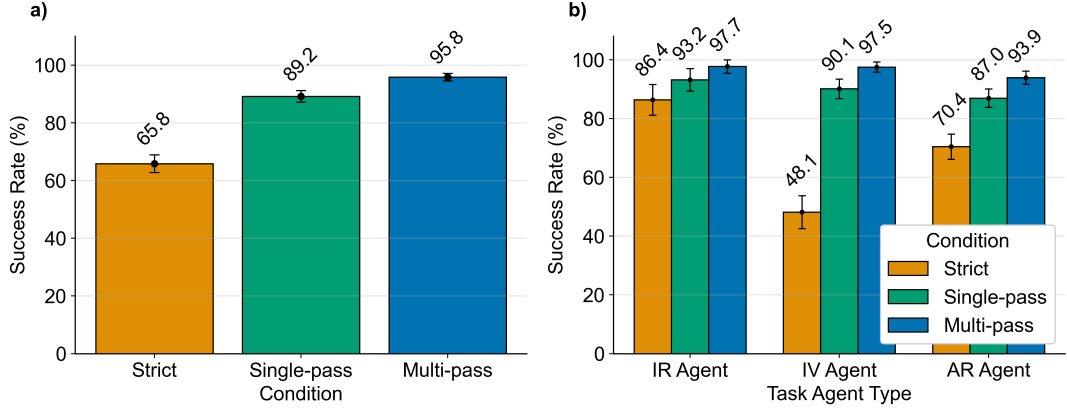


Fig. 5 Overall and task agent-specific workflow-level success rates. **a** Overall workflow-level success rate. **b** Workflow-level success rate by task agent type. Error bars in all plots indicate 95% confidence intervals.

2.3 Command-category evaluation

We evaluate the $SR_{multi-pass}$ across hierarchical command categories (Supplementary Table 1), including command structure, type, and expression as defined in Eq. (3). Overall, the SAOP handles a wide range of structural and linguistic variations in user commands (Fig. 6a). Within the command structure category, composite commands are more challenging than single commands because the platform struggles to determine the correct agent function when multiple functions must be executed sequentially. For command type category, the platform shows strong performance for explicit commands, implicit commands, and natural language questions (NLQ), demonstrating that the LLM can follow user intent with minimal performance degradation despite linguistic variations. Regarding command expression category, commands using abbreviations achieve perfect performance because the LLM prompt explicitly includes the domain-specific abbreviations. Commands with paraphrased expressions show a slightly lower performance, as such variations are not explicitly included in the prompt and may introduce additional ambiguity.

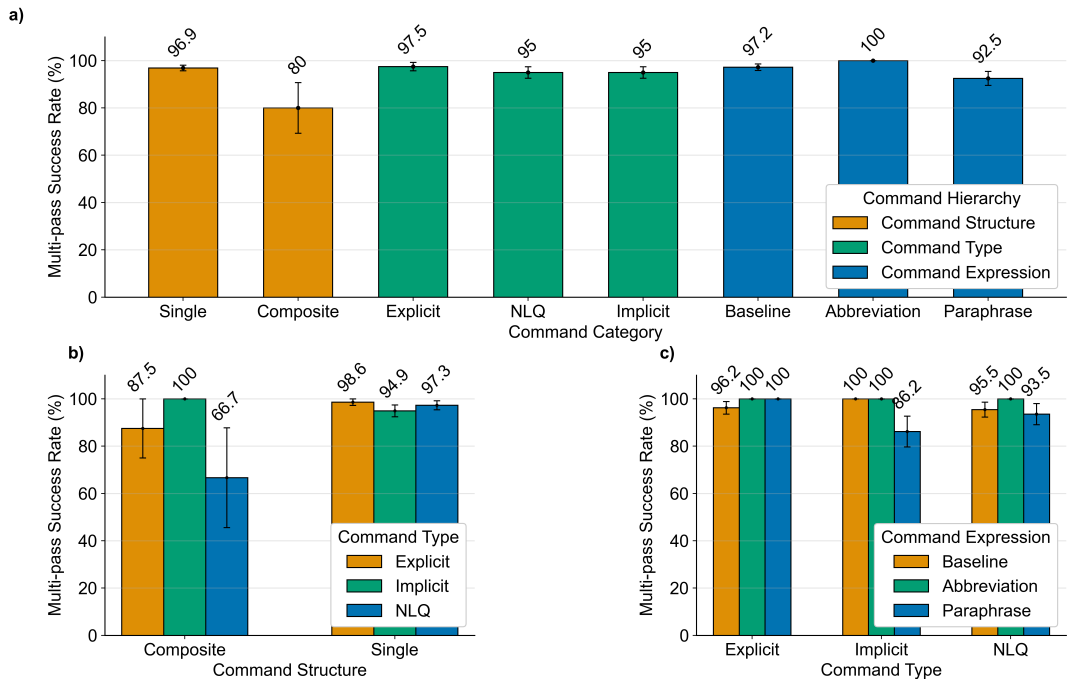


Fig. 6 Multi-pass success rate across command categories. **a** Multi-pass success rate by command category. **b** Multi-pass success rate by structure \times type. **c** Multi-pass success rate by type \times expression. Error bars in all plots indicate 95% confidence intervals.

We further analyze the hierarchical relationships among command categories using Eq. (4). In the structure–type relationship, single commands consistently achieve higher success rates than composite ones (Fig. 6b). Among composite commands, failures occur only in three cases that require chaining multiple actions, such as “Can you zoom in and rotate to the left?”, “Can you initialize and zoom in?”, or “Rotate right and zoom out”. In contrast, all command types under the single structure maintain high $SR_{multi-pass}$, demonstrating that the SAOP reliably processes straightforward, single-step commands. In the type–expression relationship, explicit commands achieve strong performance across all expression forms (Fig. 6c). This results from the explicit nature of these commands, which clearly specify both the subject (target data or agent) and the verb (intended manipulation), as well as guidance on abbreviations and some paraphrased forms in the prompt. Only two failures occur: one when the STT or correction stage fails to produce a valid command, and another involving a composite command. Implicit commands show lower robustness to unseen synonyms or paraphrases but still maintain a reasonable $SR_{multi-pass}$. Of the four failures, three are due to the platform rejecting the command as invalid, and one results from misinterpreting “pre-existing condition” and displaying both “comorbidities” and “diagnosis”. NLQs perform slightly better with paraphrase expressions because they usually contain richer contextual detail than short and implicit commands. Two failures appear: one when the platform interprets “Could you reduce coronal image?” as adjusting slice position instead of zooming out, and another when it interprets “Can you view the superior angle?” as rotating upward rather than switching to the superior view. For NLQs with baseline expressions, failures occur only in composite commands, which the platform does not currently support. These results show that SAOP generalizes well across different categories, with performance decreasing for composite or paraphrased commands that require multi-action execution and deeper reasoning on unseen expressions.

We further investigate the successful cases among challenging categories, composite commands and commands in paraphrase format. For composite commands, the IR agent retrieves all requested data in cases like “show physical and PFT info” and “show surgery and tumor information”. The IV agent accurately executes commands like “move axial to the middle slice and zoom in” or “sagittal to the center slice and zoom in”, computing mid-slice positions automatically with zoom in action, and correctly handles multi-plane commands such as “move to axial 230, coronal 220, sagittal 220” or “move to 10, 20, 50” even without explicit plane order. The AR agent correctly executes composite commands like “view from the front and rotate left” or “view from the posterior and rotate right”, when a single function can handle both actions through parameter adjustment. For paraphrased commands, we examine cases where such expressions are not explicitly defined in the prompt but convey semantically similar meanings. The IR agent can handle expressions such as retrieving the age for “How old is the patient?” and the sex for “What’s the gender?”. The IV agent interprets various expressions, executing commands like “Move front front front”, “Move left left left left”, and “Move down down” as movements to “Coronal plus 30”, “Sagittal minus 40”, and “Axial minus 20”. As the prompt defines the default movement distance for 10 units, the LLM infers the repetitions to multiples of that distance. It also predicts positions correctly for “Coronal to maximum”, “minimum”, and “middle slice”, and adapts to unseen verbs such as “step” or “slide”. For zoom operations, it performs “Zoom in” and “Zoom out” correctly for paraphrases like “Coronal enlarge,” “Focus on coronal plane,” or “Return to smaller view.” The AR agent recognizes “Add airway” as the trachea and bronchia, sets the anterior view for “look from the front,” and correctly interprets unseen synonyms for rotation and zoom actions. Overall, these results show that the LLM handles synonymous and paraphrased expressions with strong linguistic flexibility.

2.4 Applicability for real surgical settings

In surgical environments, voice characteristics differ across speakers in tone, accent, speech rate, and pronunciation. To evaluate robustness to speaker variability, we compare four synthesized neural voices with human speech. Synthesized voices achieve higher STT accuracy due to their clear and native-like pronunciation, whereas human speakers recover more effectively during invalid loops by restating the command more clearly and emphasizing key information (Fig. 7a). Although some reasoning errors occur during AD stage, all voice types maintain high stage-level accuracy. The workflow-level SR under strict, single-pass, and multi-pass conditions exhibit similar trends (Fig. 7b). The human speech exhibits lower SR_{strict} because of STT failures, but ultimately achieves the highest $SR_{multi-pass}$ as the platform recovers from invalid commands. These results demonstrate that SAOP maintains stable performance across diverse voice conditions.

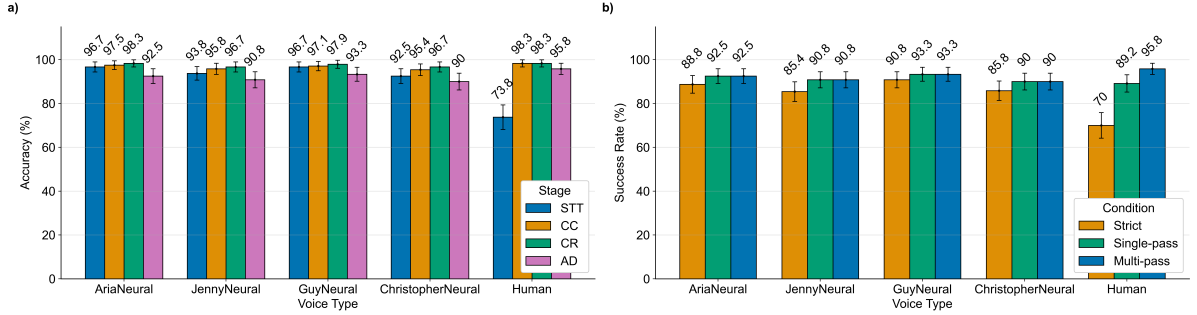


Fig. 7 The performance comparison by voice type. a Stage-level accuracy by voice type. **b** Success rate by voice type. Error bars in all plots indicate 95% confidence intervals.

Furthermore, the operating room contains background noise and conversations from multiple surgeons and nurses. To ensure that wake-word “davinci” detection does not activate accidentally, we evaluate 15 unsupported command examples (Supplementary Note 2; Supplementary Table 2). During one hour of testing, the platform records a false alarm rate of 0, indicating no unintended activations. After the wake word “davinci” is triggered, we also verify whether these examples are correctly classified as invalid. Three are misclassified as valid patient information requests, asking about vital CO_2 pressure, and frozen section. Overall, the SAOP reliably distinguishes task-related commands from unsupported commands, though a few cases suggest room to refine the command validation prompt.

2.5 Analysis of sequential command execution

We then explore scenarios to examine whether the SAOP maintains continuity across sequential video clips through memory state (<https://helena-lena.github.io/SAOP/>; Supplementary Fig. 1; Supplementary Fig. 2; Supplementary Fig. 3). The IV agent continuously updates the slice positions in sagittal, coronal, and axial views without violating the predefined minimum and maximum positional constraints. The prompt defines these guidelines and constraints, and the results show that SAOP consistently satisfies them throughout sequential updates. For the AR agent, maintaining continuity in zoom operations is particularly crucial. When multiple zoom in commands occur, the platform accurately computes the starting and ending scales while maintaining the minimum scale constraint of 1. The rotation and view adjustments also function correctly within the zoomed state, and the zoom out action follows the exact reverse path of zoom in. Additionally, when no command appears in the target video clip, the CC stage revises the empty command to “Select agent”, and the AD stage restores the previous agent state. The IR agent preserves its function and column fields, and the IV agent keeps the function, display mode, main view, and slice positions. If the previous clip involved rotation, zoom, or a static action, the AR agent sets agent function to “show static recon” while retaining all other state parameters. For the “Reset” command, each agent restores the default settings of agent function and parameters defined in the prompt. These results demonstrate that our voice-directed SAOP preserves temporal and functional consistency across video clips, ensuring stable and continuous state transitions.

3 Discussion

We demonstrate the effectiveness of the hierarchical multi-agent framework with LLM-based orchestration. The workflow orchestrator agent reliably plans and selects appropriate functions based on the current state and predefined decision rules. The hybrid design of LLM-driven reasoning with probability-based decision rules resolves invalid loops and enables workflow stages to progress smoothly. Although computing probabilities for all functions slows inference compared to direct function prediction, it could enable conditional probability-based planning to handle increasingly complex paths as the number of agents and functions grows. Separating workflow functions from task-specific agent functions further improves modularity and scalability, allowing flexible integration of new agents or functions. Expanding clinically useful agents, such as detecting critical blood vessels, supporting intraoperative navigation, and assisting in robotic planning, will enhance the clinical applicability of our voice-directed SAOP.

While our platform demonstrates the feasibility of LLM-based orchestration for surgical assistance, the observed errors reveal opportunities for improvement. At the STT stage, most errors occur with medical domain-specific terminology, suggesting the need to fine-tune lightweight STT models on medical terms to improve transcription accuracy. In the CC stage, the LLM revises misrecognized words to their intended medical terms, yet augmenting text correction rules or fine-tuning a correction model on medical context could further enhance robustness in failure cases. At the AD stage, most errors arise from composite commands, indicating the need to extend the SAOP to support multi-step sequential operations. Additionally, since the current prompting strategy are closely coupled with the Gemma3 [22] model, performance may vary across different LLMs. Developing a self-evolving orchestration mechanism that learns from prior errors and dynamically refines its prompts could ensure adaptability and consistent performance across models in future implementations.

From a dataset perspective, the evaluation uses 240 commands that include both human and synthesized voice inputs from four different speakers to simulate variability. However, the dataset still lacks the diversity of speaking styles, terminology preferences, and phrasing observed in real clinical settings. In practice, commands often contain a mix of multiple languages, medical terms in English while the rest of the command is spoken in the native language. To ensure accurate STT performance under such multilingual and domain-specific conditions, future work may involve fine-tuning models on multilingual medical data or integrating fast and commercially available multilingual speech recognition systems. Moreover, the clinical information displayed by the IR agent is based on a predefined set of columns selected by clinicians. However, the required fields may vary across departments and individual surgeons, indicating the need for customizable data configurations. For 3D anatomical models displayed by AR agent, using commercial or clinically validated software could provide more precise anatomical structures and support more sophisticated manipulation for clinical use.

In terms of computational efficiency, we employ gemma3:27b-it-qat for LLM model, a quantization-aware trained version that preserves high performance while reducing memory usage (Supplementary Note 3). This model runs within 17 GB of GPU memory, and our server is equipped with two NVIDIA RTX 4500 Ada GPUs (24GB), allowing local and efficient inference. The cumulative inference latency from sequential LLM calls presents a usability challenge in time-sensitive surgical environments. This delay becomes more pronounced when the LLM engages in complex reasoning or generates longer outputs. Inference time can be reduced by applying LLM reasoning only to essential stages and omitting it in stages that have little effect on overall performance. To mitigate this issue, the platform can incorporate techniques such as reasoning-pattern caching, strategies to shorten LLM output length, and adaptation to surgeon-specific patterns to reduce overall processing delays. For the 3D model overlay on surgical videos, increasing mesh decimation or frame skipping can improve rendering speed, but may result in less smooth rotation and zoom interactions.

4 Methods

4.1 Overall Workflow

Our voice-directed SAOP is a hierarchical multi-agent framework that automatically plans and executes the overall workflow (Fig. 1; Fig. 8). We divide the surgical video into 10-second clips because it is often longer than one hour, and each clip is designed to handle a single command. The workflow orchestrator agent first initializes the memory state, consisting of a local memory state for each clip and a global memory state to ensure consecutive information sharing across clips. The agent then leverages the LLM to automatically determine the next function to execute based on the available set of functions. The input prompt to the LLM includes instructions, function names and definitions, predefined workflow decision rules, the current status, and the output format requirements (Supplementary Note 4).

We categorize the functions into two types: workflow functions and task-specific agent functions. Workflow functions are for higher-level coordination that process and analyze voice commands through voice interaction, transcription, correction, validation, and reasoning for agent routing. Task-specific agent functions operate at a lower level to select the appropriate agent function and determine the state parameters. This hierarchical design improves modularity and maintainability, allowing the platform to flexibly incorporate new agents or functions without disrupting the overall workflow.

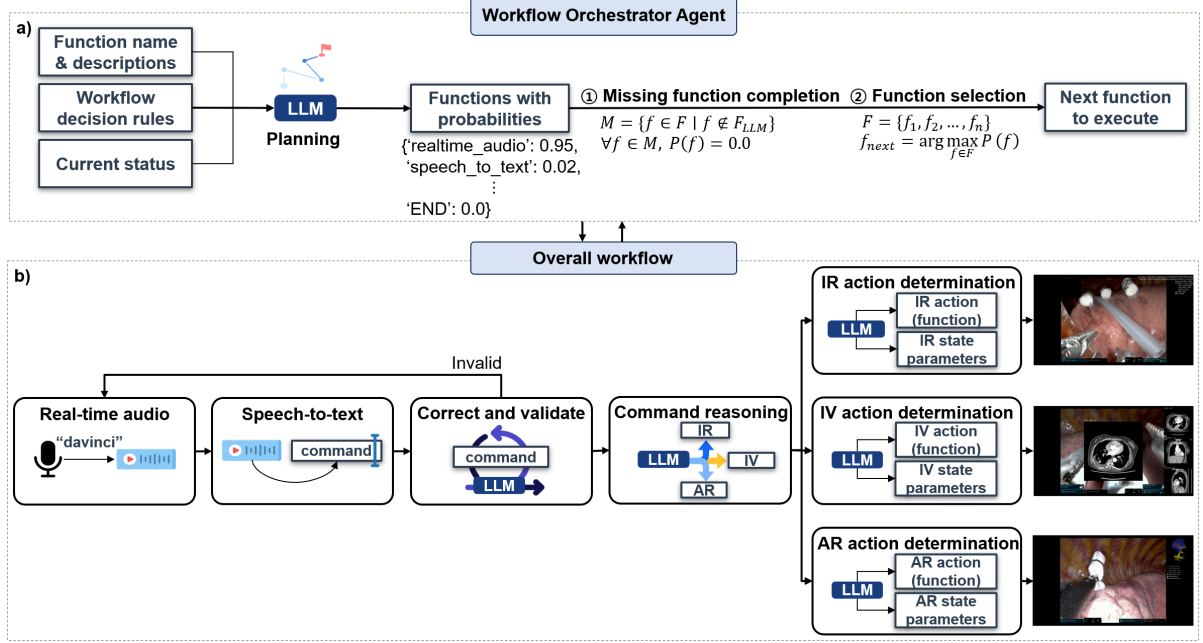


Fig. 8 Overall workflow controlled by Workflow Orchestrator Agent. **a** Hybrid approach of LLM and mathematical rules for the Workflow Orchestrator Agent. **b** Overall workflow planned by Workflow Orchestrator Agent.

In determining return points or termination, relying solely on function names and descriptions can lead to mispredictions. To mitigate this, workflow decision rules guide the overall process and define when to return and end. In addition, current status such as “No audio recorded”, “Last command invalid, need new input”, “IR Agent completed, workflow finished” provides contextual cues that help navigate branching points. The workflow decision rules and current status allow the orchestrator to make more accurate and consistent decisions across diverse scenarios.

The LLM output should be in json format, containing each function name along with its associated probability for the next step. Incorporating probabilities allows the platform to provide a quantitative measure of confidence for decision-making. Since the LLM output may omit certain functions, the missing function completion rule includes all absent functions M with their probabilities set to zero. Subsequently, the function selection rule chooses the next function f_{next} with the highest probability over the complete function set. This hybrid approach combines the capabilities of LLMs with the probability-based decision rules, ensuring reliability and mathematical grounding.

4.2 Workflow Functions

4.2.1 Real-time Audio Function

The real-time audio function manages voice interaction from capturing voice input from the local notebook to transmitting the audio file to a remote server as shown in Algorithm 1. As this function requires fast real-time processing on CPU, it integrates Silero-VAD (<https://github.com/snakers4/silero-vad>) for voice activity detection (VAD), Whisper-small model [44] via faster-whisper (<https://github.com/SYSTRAN/faster-whisper/tree/master>) for speech recognition and wake-word detection “davinci”, and Microsoft Edge TTS (<https://github.com/rany2/edge-tts>) for text-to-speech. To improve wake word detection and avoid false activation, we optimize Whisper-small decoding parameters by defining “davinci” as hotwords, setting the temperature to 0, beam size to 5, no-speech threshold to 0.25, compression ratio threshold to 1.2, and log probability threshold to -1.0 . The process starts with local notebook microphone streaming, where VAD detects speech activity, Whisper transcribes speech, identifies the wake word “davinci”, records the surgeon’s command, and transmits to the remote server.

Algorithm 1 Real-time Audio Recording and Server Transmission Pipeline

Input: Audio stream from microphone, Silero-VAD model M_{VAD} , Whisper-small model M_W , Microsoft Edge TTS model M_{TTS} , keyword set $\mathcal{K} = \{ \text{"davinci"}, \text{"davin"}, \text{"vinci"} \}$

Output: Recorded audio file transmitted to remote server

1. **Initialization:**

- Load M_{VAD} and M_W .
- Play M_{TTS} (“Ready.”)

2. **Keyword Detection (Wake-word Listening):**

- Open microphone stream S .
- Continuously read chunks x_t and compute timestamps $T = \text{VAD}(x_t)$.
- If speech detected by M_{VAD} , transcribe buffer via M_W .
- If keyword $\in \mathcal{K}$ found, play M_{TTS} (“Please continue.”) and proceed.

3. **Recording:** Record speech until 4 seconds of silence.

4. **Save and Transfer:** Save as WAV, upload via SCP

Algorithm 2 Speech-to-Text (STT) Function

Input: Workflow state \mathcal{S} containing audio path, STT model M_{STT}

Output: Transcription results (commands)

1. **Initialization:** Load audio from $\mathcal{S}[\text{audio_path}]$.

2. **Transcription:**

- Use M_{STT} to transcribe the audio
- Store each segment’s start time, end time, and text as `stt_chunks`.

3. **Command Extraction:**

- Concatenate all transcribed texts to form commands.
- If `commands = \emptyset` , set `commands = “None”`.
- Append `commands` to $\mathcal{S}[\text{commands}]$.

4. **Update workflow state:** $\mathcal{S} \leftarrow \{\text{stt_chunks}, \text{commands}\}$.

4.2.2 Speech-to-Text (STT) Function

The STT function employs the Whisper-medium model [44] integrated with faster-whisper for efficient inference. Comparing SpeechBrain model [45], the Whisper models, and Microsoft Phi-4-multimodal model [46], the Whisper-medium model offers a practical balance between speed and accuracy (Supplementary Note 5; Supplementary Fig. 4). The larger models generally achieve higher accuracy but incur slower inference. The Whisper-medium model is configured with a beam size of 8, the language parameter set to “en”, a temperature of 0, a speech threshold of 0.3, and a log prob threshold of -2.0 to enhance transcription accuracy for English speech while effectively filtering out non-speech segments and low-confidence outputs. Lastly, the transcribed command is updated in the memory state, and the overall procedure is shown in Algorithm 2.

4.2.3 Correct and Validate Function

The correct and validate function employs Gemma3 [22] LLM to correct the transcribed command and determine its validity (Fig. 9a). The prompt contains the available task agents and their descriptions, instructions, command correction rules, validation rules, output format, memory state, and current transcribed command (Supplementary Note 6). The instruction first requests to translate the command into English and apply appropriate revisions. Since the STT model is unfamiliar with medical terminology such as axial, coronal, posterior, and CT, we provide text correction rules to handle such failure cases. For example, “Replace ‘city’ with ‘CT’” and “Replace COVID-related terms with ‘coronal’”. Ambiguity

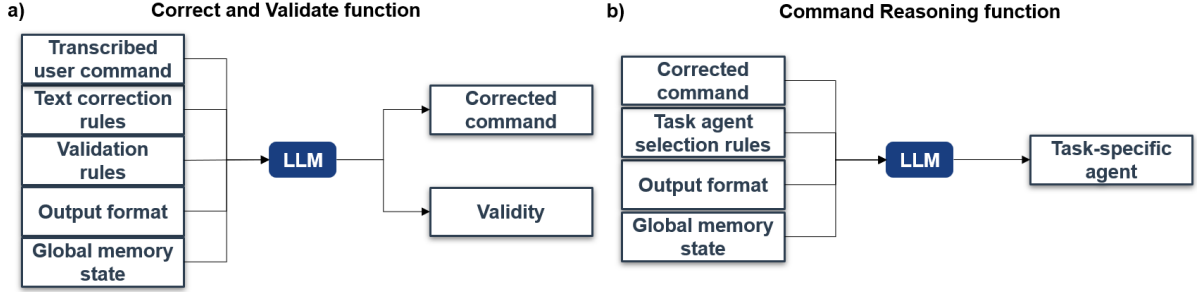


Fig. 9 The input and output of correct and validate function and command reasoning function. **a** The correct and validate predicts the corrected command and its validity. **b** The command reasoning prompt determines the most appropriate task-specific agent. Both functions leverage previous commands and agent history from global memory state, and step-by-step CoT reasoning.

also arises with commands like zoom in/out, which may refer either to the IV agent or the AR agent. To resolve these issues, the prompt incorporates the memory state by providing the last three revised commands and associated agents. The LLM then outputs a json containing the corrected command and its validity, which is updated in the memory state. Valid commands are ready to proceed to the command reasoning function for further processing, whereas invalid ones should return to the real-time audio function for a new voice input. In addition, when the command is “None”, the platform automatically inherits the action from the previous video clip, and thus LLM revises as “Select {agent name}”.

4.2.4 Command Reasoning Function

The command reasoning function takes the revised command as input and employs Gemma3 model to reason and select the most appropriate task agent (Fig. 9b). The prompt includes the available task agents with brief descriptions, instructions, memory state, and the current revised command (Supplementary Note 7). As in the correct and validate function, providing the last three revised commands and corresponding agents aids in resolving ambiguous commands. We apply Chain-of-Thought (CoT) prompting [23] for the reasoning process, which are helpful to analyze error cases and refine detailed agent descriptions according to them. The model finally returns a json object specifying the name of the selected agent, which is also updated in the memory state.

4.3 Task-specific Agent Functions

4.3.1 Information Retrieval (IR) Agent Functions

The IR agent overlays the requested clinical data on the surgical video (Fig. 10; Supplementary Fig. 5). It comprises three functions: an action determiner (AD) function that interprets commands and decides the action and parameters, and two functions for showing or removing the overlay. The AD function leverages Gemma3 to infer the action uniquely mapped to an agent function and state parameters (Supplementary Note 8). We denote the command by $x \in \mathcal{X}$, the instruction by i , and a set of patient-data columns by $\mathcal{C} = \{c_1, \dots, c_m\}$ with corresponding values $v = \{v_1, \dots, v_m\}$. The LLM parameterized by θ produces an action distribution π_θ over $\{\text{SHOW}, \text{HIDE}\}$ and a per-field inclusion probability ϕ_θ :

$$\begin{aligned} \pi_\theta(a | x, i) &= \Pr(A = a | x, i), \\ \phi_\theta(j | x, i, a) &= \Pr(Y_j = 1 | x, i, a), \quad j = 1, \dots, m. \end{aligned} \quad (5)$$

The agent selects the action a^* with the higher probability and predicts the indicator vector $y^* \in \{0, 1\}^m$ that specifies which fields to display, as formulated in Equation 6. To handle ambiguous expressions like physical information, the prompt guides their mapping to specific fields in \mathcal{C} , adjusting the ϕ_θ .

$$\begin{aligned} a^* &= \arg \max_{a \in \{\text{SHOW}, \text{HIDE}\}} \pi_\theta(a | x, i), \\ y_j^* &= \mathbf{1}[\phi_\theta(j | x, i, a^*) \geq \tau], \quad j = 1, \dots, m. \end{aligned} \quad (6)$$

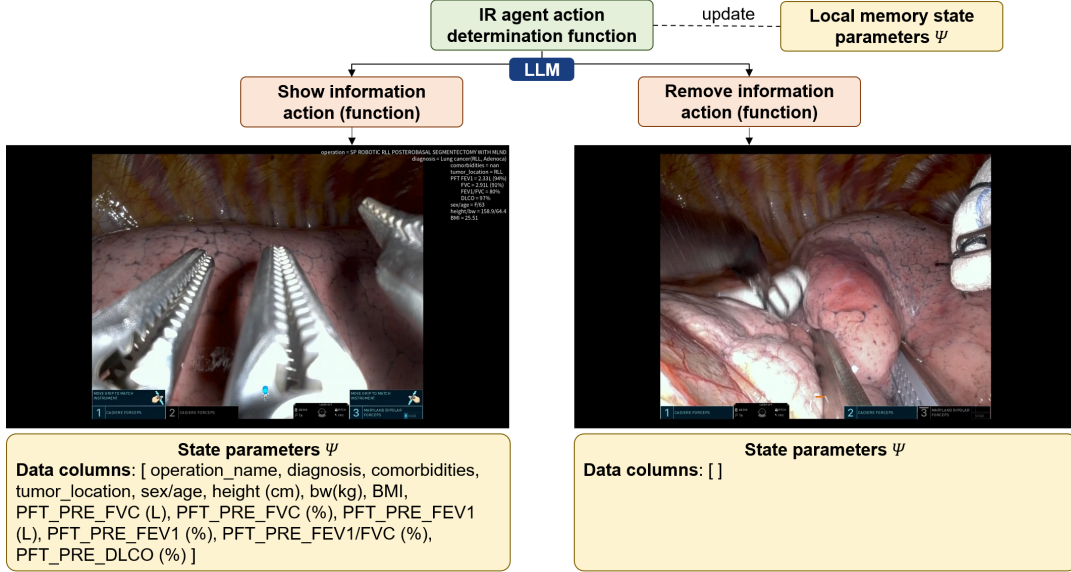


Fig. 10 The overview of the IR agent. The LLM in the action determination function predicts the action and its state parameters, and the IR agent then executes either the show or remove function with inferred parameters.

The state parameters of the IR agent are defined as:

$$\Psi = (y, s), \quad \begin{aligned} y &\in \{0, 1\}^m, \\ s &\in \text{final string}. \end{aligned} \quad (7)$$

Here, y denotes the binary indicator vector specifying which data fields are active, and s is the final patient information string to overlay. When $a^* = \text{HIDE}$, the agent sets $y^* = \mathbf{0}$ and assigns an empty string s . When $a^* = \text{SHOW}$, the agent retrieves the relevant clinical data and formats it according to physician preferences to construct s . Given the indicator vector y^* , the subset of columns to display is:

$$\mathcal{C}_{y^*} = \{c_j \in \mathcal{C} \mid y_j^* = 1\}. \quad (8)$$

For each selected column $c_j \in \mathcal{C}_{y^*}$ with value v_j , a field-specific formatting function $r(c_j, v_j)$ transforms the raw data into a textual representation.

$$r(c_j, v_j) : (c_j, v_j) \mapsto \text{string}, \quad c_j \in \mathcal{C}_{y^*}. \quad (9)$$

This formatting function reflects physician feedback, such as combining pulmonary function test values in liters and percentages, merging relevant fields like sex and age, and omitting unnecessary units. The final patient information string is the result of concatenating all the formatted outputs with newline delimiters.

$$s = \text{concat}_{c_j \in \mathcal{C}_{y^*}} r(c_j, v_j), \text{ delimiter} = "\backslash n". \quad (10)$$

Finally, the SHOW action links to a display function that overlays the generated text on the top-right corner of each video frame. In contrast, the HIDE action connects to a removal function that restores the original frame without any overlay. Given a sequence of video frames $\{I_t\}_{t=1}^T$ and an overlay box position p , the overlay operator \mathcal{O}_{IR} places the patient information string s on each frame as follows:

$$\tilde{I}_t = \mathcal{O}_{IR}(I_t; s, p), \quad t = 1, \dots, T. \quad (11)$$

The selection of data columns and the visual presentation style is refined through continuous consultation with clinicians to ensure readability.

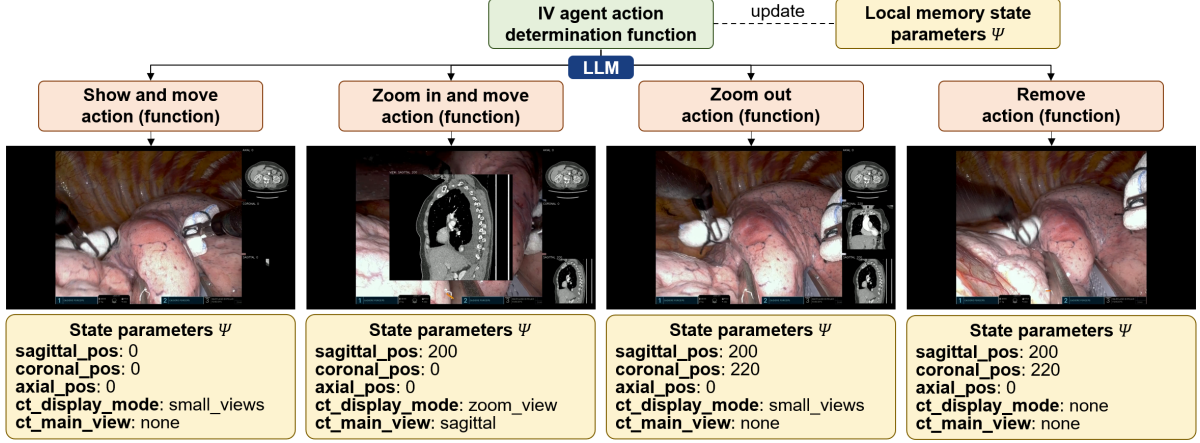


Fig. 11 The overview of the IV agent. The action determination function predicts the action and state parameters, and the IV agent executes show, zoom in, zoom out, or remove function with inferred parameters.

4.3.2 Image Viewer (IV) Agent Functions

The IV agent overlays CT DICOM images onto the surgical video, allowing surgeons to scroll through axial, coronal, and sagittal planes (Fig. 11; Supplementary Fig. 2). The AD function interprets commands to manipulate CT slices with four functions: displaying and moving multi-planar views, zooming into a large single view, zooming out to the small multi-planar views, and removing all CT views. We denote the command $x \in \mathcal{X}$, the instructions by i , and the state parameters by Ψ . The Gemma3 model parameterized by θ infers the action $A \in \mathcal{A}$, $\mathcal{A} = \{\text{SHOW_MOVE}, \text{ZOOM_IN_MOVE}, \text{ZOOM_OUT}, \text{REMOVE}\}$ and updates the state parameters Ψ (Supplementary Note 9). The decision process follows a joint policy that factorizes into an action selection policy and a state update policy:

$$\begin{aligned} \pi_\theta(a, \Psi | x, i) &= \pi_\theta(a | x, i) \pi_\theta(\Psi | x, i, a), \\ a^* &= \arg \max_{a \in \mathcal{A}} \pi_\theta(a | x, i), \\ \Psi^* &= \arg \max_{\Psi} \pi_\theta(\Psi | x, i, a^*), \end{aligned} \quad (12)$$

The policy first infers the action a^* , and then predicts the updated state parameters Ψ^* conditioned on that action. The Ψ denotes the current state and Ψ^* is the updated state after adjustments.

Specifically, the state parameters are defined as $\Psi = (p, \delta, v)$, where $p = (p^{\text{axi}}, p^{\text{cor}}, p^{\text{sag}})$ denotes the slice positions, $\delta \in \{\text{none}, \text{small_views}, \text{zoom_view}\}$ is the display mode, and $v \in \{\text{axial}, \text{coronal}, \text{sagittal}\}$ is the main view plane. The slice positions are updated based on movement commands:

$$p^* = p + \Delta p(x, i, a^*), \quad (13)$$

where Δp encodes positional adjustments such as “move right” or “sagittal plus 50” (increase sagittal index), “move down” or “axial minus 100” (decrease axial index), and “move forward” or “coronal plus 30” (increase coronal index). The display mode δ determines how CT slices appear on the surgical video. If a^* is SHOW_MOVE, δ is small_views, showing three CT views $I_t^{\text{axi}}, I_t^{\text{cor}}, I_t^{\text{sag}}$ on the right side of the video, each with the updated positions p^* . If a^* is ZOOM_IN_MOVE, δ is zoom_view, displaying a main CT view I_t^{main} in the center of the video. The main view v is either explicitly specified in the command or implicitly inferred from the movement axis: $I_t^{\text{main}} = \mathcal{V}(p^*, v)$. If $a^* = \text{ZOOM_OUT}$, δ is small_views, removing the main CT view and keeping the small views visible. If $a^* = \text{REMOVE}$, δ is none, which removes all CT views.

Given video frames $\{I_t\}_{t=1}^T$, action a^* , and the updated state Ψ^* , the overlay operator generates

$$\tilde{I}_t = \mathcal{O}_{IV}(I_t; p^*, a^*, \delta, v), \quad t = 1, \dots, T. \quad (14)$$

To ensure smooth transitions, \mathcal{O}_{IV} interpolates slice positions from p to p^* over five seconds.

4.3.3 Anatomy Rendering (AR) Agent Functions

The AR agent renders 3D anatomical models on the surgical video to enable interactive visualization (Fig. 12; Supplementary Fig. 3). The 3D models are reconstructed from CT images using TotalSegmentator (<https://github.com/wasserth/TotalSegmentator>) in the 3D Slicer (<https://www.slicer.org/>), software which generates segmented anatomical structures with corresponding labels. The AD function interprets commands and selects one of five actions: displaying static views, rotating the model, zooming in on specific structures, zooming out, and removing all models. Given a command $x \in \mathcal{X}$, instructions i , and the current state parameters Ψ , the Gemma3 LLM jointly infers the action $A \in \mathcal{A}$, $\mathcal{A} = \{\text{STATIC}, \text{ROTATE}, \text{ZOOM_IN}, \text{ZOOM_OUT}, \text{REMOVE}\}$ and updates the state parameters Ψ (Supplementary Note 10). The decision process follows the same joint policy formulation Equation 12 as in the IV agent. The key difference is that the actions, the state parameters, and the instructions to update them are all specific to the AR Agent. Specifically, the state parameters include active anatomical structures α , viewpoint v , rotation mode r , target structure for zoom τ , and zoom parameters z .

The active anatomical structures α represent the list of visible structures. The physician selects the anatomical labels of interest, including left lower lobe, left upper lobe, right lower lobe, right middle lobe, right upper lobe, lung nodules, and the trachea/bronchia. The default setting activates only the lobe with nodules and all non-lobe structures. The LLM applies this default configuration when the command first invokes the AR agent, resets, or requests to show the surgical part. Subsequent commands that add or remove structures update α , whereas commands that do not mention structure leave α unchanged.

The viewpoint $v \in \{\text{anterior}, \text{posterior}, \text{left}, \text{right}, \text{superior}, \text{inferior}, \text{surgical}\}$ specifies the initial view of the 3D model. For example, commands such as “Show the anterior view” or “Show from the front” display the anterior side. In rotation commands, such as “Rotate the posterior view to the left”, the initial viewpoint v is set to the posterior view. The default viewpoint is set to surgical view, which aligns to the perspective of a patient lying on the operating table, as illustrated in Figure 12.

The rotation mode $r \in \{\text{static}, \text{left}, \text{right}, \text{up}, \text{down}, \text{horizontal}, \text{vertical}\}$ is the relative rotation direction from the initial viewpoint v . The static mode does not rotate the model, left/right/up/down modes rotate 30 degrees toward the specified direction and returns to the original view, and the horizontal/vertical modes perform a continuous 360 degrees rotation. The default setting is the static mode and clinicians can rotate the model in desired directions to inspect critical regions for resection.

If a^* is ZOOM_IN or ZOOM_OUT, the LLM extracts the target structure τ from the command and updates the zoom parameters $z^* = (z_c^*, z_s^*, z_\ell^*)$, where z_c^* is the center of τ , z_s^* is the zoom scale, and z_ℓ^* is the zoom depth level. The zoom in operation moves toward z_c^* and stores the zoom path in a history

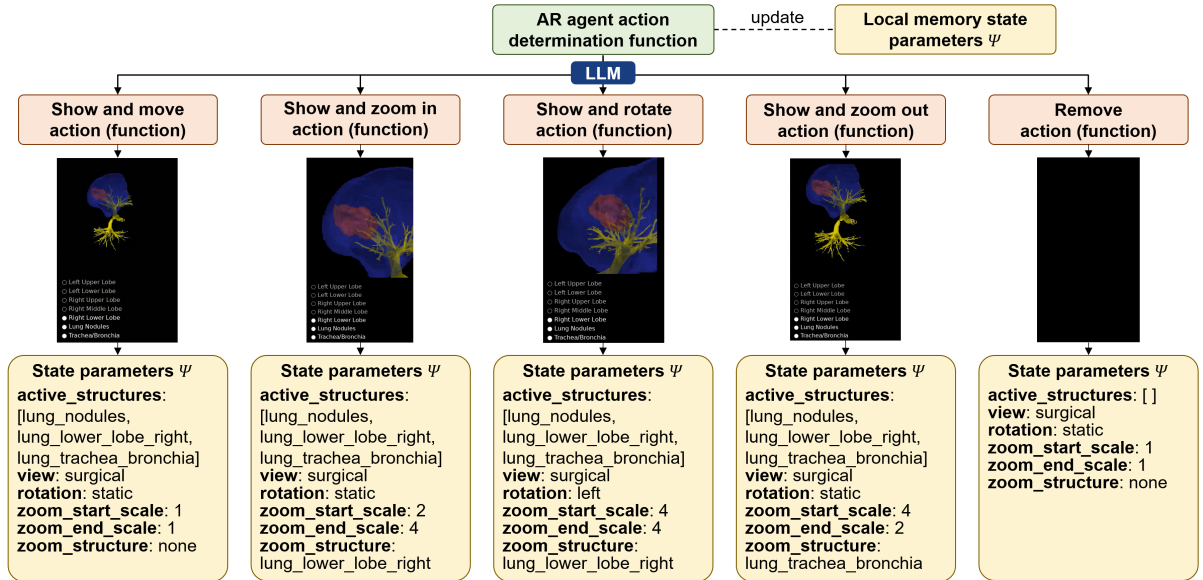


Fig. 12 The overview of the AR agent. The action determination function predicts the action and state parameters, then the AR agent executes static, zoom in, rotate, zoom out, or remove function with predicted parameters.

stack, which is later traversed in reverse order during the zoom out operation. The zoom scale z_s has three values: start scale z_s^{start} , end scale z_s^{end} , and the actual current scale z_s^{current} . Specifically,

$$\begin{aligned} \text{rotate/static: } z_s^{\text{start}} &= z_s^{\text{end}} = z_s^{\text{current}}, \\ \text{zoom in: } z_s^{\text{start}} &= z_s^{\text{current}}, \quad z_s^{\text{end}} = 2z_s^{\text{current}} \\ \text{zoom out: } z_s^{\text{start}} &= z_s^{\text{current}}, \quad z_s^{\text{end}} = \max(1.0, \frac{1}{2}z_s^{\text{current}}). \end{aligned} \quad (15)$$

The scale starts at $z_s = 1.0$, doubling with each zoom in and halving with each zoom out until the minimum scale of 1.0. The zoom depth level z_ℓ increases for zoom in and decreases for zoom out.

Given video frames $\{I_t\}_{t=1}^T$, action a , and updated state Ψ^* , the overlay operator \mathcal{O}_{AR} generates

$$\tilde{I}_t = \mathcal{O}_{\text{AR}}(I_t; \Psi^*, a^*), \quad t = 1, \dots, T. \quad (16)$$

To ensure visual smoothness, \mathcal{O}_{AR} interpolates the rotation and zoom transitions across frames. Zoom operations complete within three seconds, left/right/up/down rotation within seven seconds (three seconds movement, one second hold, 3 seconds return), and horizontal/vertical rotation within six seconds. The resulting overlays appear in the upper-right corner of the surgical video, allowing the surgeon to identify critical structures that require attention during the procedure.

4.4 Dataset

We construct a command dataset consisting of 240 user commands to evaluate our voice-directed SAOP. Among them, 44 commands belong to the IR agent, 81 commands correspond to the IV agent, and the remaining 115 commands are associated with the AR agent (Supplementary Table 3). This distribution reflects the diverse functional load of each agent. The AR agent accounts for nearly half of all commands because it offers a broader range of actions for 3D model interaction.

Each command also includes category annotations along three hierarchical dimensions: command structure, command type, and command expression (Supplementary Table 1). In the command structure dimension, single command contains one clearly defined action or data request, while composite command combines two or more actions or data requests. These composite command includes multi-action requests such as “move axial to the middle slice and zoom in”, and multi-data requests like “show physical and PFT info.”

The command type dimension classifies each command as explicit command, implicit command, or NLQ, reflecting the varying levels of linguistic clarity and ambiguity. Explicit command clearly state both the subject (the target data or agent) and the verb (the action), forming a grammatically complete and semantically clear instruction. These commands typically match the phrasing defined in the prompt instructions and do not require additional contextual reasoning such as “Show patient information”. Implicit command omit either the subject or the verb, making them grammatically incomplete and dependent on prior memory context. They often appear in continuous interactions where users skip information already mentioned in earlier commands. For example, users may omit the subject in “Zoom in”, “Initialize”, or “Rotate to the right”, or omit the verb as “Diagnosis” or “Surgical view”. The LLM should interpret such commands by leveraging previous memory states and contextual cues. NLQ take the form of questions, using conversational QA-style phrasing. Examples include “How old is the patient?”, “Can you magnify the sagittal view?”, and “Can you activate the right lung?”.

Finally, the command expression dimension characterizes lexical variations, indicating whether the command follows the baseline form, includes abbreviations, or paraphrases. Baseline command is the canonical form of expressions without any abbreviations or paraphrased expressions. Commands with abbreviations include medical terms such as PFT (Pulmonary Function Test) or RUL (Right Upper Lobe) that require domain knowledge, as well as general abbreviations like info (information). Commands with paraphrased expressions express the same intent as baseline commands but use alternative synonyms or phrasings. Because clinicians may prefer different terminology or phrasing styles, this category evaluates linguistic flexibility and contextual understanding. Examples include “Move front, front, front” (Coronal plus 30), “Coronal view to the middle slice” (Move coronal to 256), “Show from the front” (Show from the anterior), and “Rotate left and right” (Rotate horizontally).

We additionally synthesize voice command datasets for four different speakers using Microsoft Edge TTS that we use in real-time speech function. Among the available voices, we select two female and two male speakers categorized under “News”, as they are native English speakers and provide clear pronunciation. Specifically, en-US-AriaNeural conveys polite and confident tones, en-US-JennyNeural sounds friendly, considerate, and comforting, en-US-GuyNeural expresses passion, and en-US-ChristopherNeural reflects reliability and authority.

Patient data comes from the department of thoracic and cardiovascular surgery at Korea University Guro Hospital, involving a patient who had lung surgery using the Da Vinci robotic system. The patient data encompass surgical videos, clinical information, CT images, and 3D anatomical structure models. This study is ethically approved by the Institutional Review Board at Korea University Guro Hospital (IRB No. 2025GR0018), and informed consent was waived due to its retrospective design of the study.

5 Data availability

The command dataset (xlsx format) is provided in the Supplementary Data 1 file, and the synthesized voice command datasets (mp3 format) are available in the Github repository: <https://github.com/helena-lena/SAOP>. The de-identified patient data is not publicly available due to the privacy laws, specifically the Personal Information Protection Act of the Republic of Korea.

6 Code availability

The codes for the proposed voice-directed SAOP used in this study is available at the following GitHub repository: <https://github.com/helena-lena/SAOP>.

7 Acknowledgments

This research was supported by a grant of the Korea Health Technology R&D Project through the Korea Health Industry Development Institute (KHIDI), funded by the Ministry of Health & Welfare, Republic of Korea (grant number: RS-2024-00436472). Additionally, this work was supported by the National Research Foundation of Korea (NRF) grant, funded by the Korea government (MSIT)(grant number: RS-2025-00518091).

8 Author contributions

H.P. implemented the system, conducted all experiments, analyzed the results, and drafted the manuscript. B.M.G., and J.H.L. collected the data and provided clinical feedback. B.H.C. managed the server for data storage and processing. S.K. advised on system implementation and evaluation, and contributed to manuscript preparation. H.K.K., and K.K. supervised the project from conceptualization to discussion, and contributed to manuscript preparation.

9 Competing interests

All authors declare no financial or non-financial competing interests.

References

- [1] Allaf, M. E. et al. Laparoscopic visual field: voice vs foot pedal interfaces for control of the aesop robot. *Surg Endosc*, **12**, 1415–1418 (1998).
- [2] Mettler, L., Ibrahim, M. & Jonat, W. One year of experience working with the aid of a robotic assistant (the voice-controlled optic holder aesop) in gynaecological endoscopic surgery. *Hum Reprod*, **13**, 2748–2750 (1998).
- [3] Reichenspurner, H. et al. Use of the voice-controlled and computer-assisted surgical system zeus for endoscopic coronary artery bypass grafting. *J Thorac Cardiovasc Surg*, **118**, 11–16 (1999).

- [4] Nathan, C. O., Chakradeo, V., Malhotra, K., D’Agostino, H. & Patwardhan, R. The voice-controlled robotic assist scope holder aesop for the endoscopic approach to the sella. *Skull Base*, **16**, 123–131 (2006).
- [5] Salama, I. A. & Schwaitzberg, S. D. Utility of a voice-activated system in minimally invasive surgery. *J Laparoendosc Adv Surg Tech*, **15**, 443–446 (2005).
- [6] Vaida, C. et al. Development of a voice controlled surgical robot. *New Trends in Mechanism Science: Analysis and Design* 567–574 (Springer, 2010).
- [7] Forte, M. P. et al. Design of interactive augmented reality functions for robotic surgery and evaluation in dry-lab lymphadenectomy. *Int J Med Robot*, **18**, e2351 (2022).
- [8] Elazzazi, M., Jawad, L., Hilfi, M. & Pandya, A. A natural language interface for an autonomous camera control system on the da vinci surgical robot. *Robotics*, **11**, 40 (2022).
- [9] Kim, Y. G. et al. Speech-mediated manipulation of da vinci surgical system for continuous surgical flow. *Biomed Eng Lett*, **15**, 117–129 (2025).
- [10] Davila, A., Colan, J. & Hasegawa, Y. Voice control interface for surgical robot assistants. In *2024 International Symposium on Micro-NanoMechatronics and Human Science (MHS)* 1–5 (IEEE, 2024).
- [11] Pandya, A. Chatgpt-enabled davinci surgical robot prototype: advancements and limitations. *Robotics*, **12**, 97 (2023).
- [12] Zhang, Y., Orthmann, B., Welle, M. C., Van Haastregt, J. & Kragic, D. Llm-driven augmented reality puppeteer: Controller-free voice-commanded robot teleoperation. In *International Conference on Human-Computer Interaction* 97–112 (Springer, 2025).
- [13] Gavric, A., Bork, D. & Proper, H. A. Surgery ai: Multimodal process mining and mixed reality for real-time surgical conformance checking and guidance. *ZEUS 2025*, 48 (2025).
- [14] Achiam, J. et al. Gpt-4 technical report. *arXiv preprint arXiv:2303.08774* (2023).
- [15] Chowdhery, A. et al. Palm: Scaling language modeling with pathways. *J Mach Learn Res*, **24**, 1–113 (2023).
- [16] Touvron, H. et al. Llama: Open and efficient foundation language models. *arXiv preprint arXiv:2302.13971* (2023).
- [17] Touvron, H. et al. Llama 2: Open foundation and fine-tuned chat models. *arXiv preprint arXiv:2307.09288* (2023).
- [18] Dubey, A. et al. The llama 3 herd of models. *arXiv e-prints*, arXiv–2407 (2024).
- [19] Meta AI. The llama 4 herd: The beginning of a new era of natively multimodal ai innovation. <https://ai.meta.com/blog/llama-4-multimodal-intelligence/> (2025).
- [20] Gemma Team. Gemma: Open models based on gemini research and technology. *arXiv preprint arXiv:2403.08295* (2024).
- [21] Gemma Team. Gemma 2: Improving open language models at a practical size. *arXiv preprint arXiv:2408.00118* (2024).
- [22] Gemma Team. Gemma 3 technical report. *arXiv preprint arXiv:2503.19786* (2025).

- [23] Wei, J. et al. Chain-of-thought prompting elicits reasoning in large language models. In *Advances in Neural Information Processing Systems*, Vol. 35 24824–24837 (NeurIPS, 2022).
- [24] Wang, X. et al. Self-consistency improves chain of thought reasoning in language models. *arXiv preprint arXiv:2203.11171* (2022).
- [25] Yao, S. et al. Tree of thoughts: Deliberate problem solving with large language models. In *Advances in neural information processing systems*, Vol. 36 11809–11822 (NeurIPS, 2023).
- [26] Besta, M. et al. Graph of thoughts: Solving elaborate problems with large language models. In *Proceedings of the AAAI conference on artificial intelligence*, Vol. 38 17682–17690 (AAAI, 2024).
- [27] Franklin, S. & Graesser, A. Is it an agent, or just a program?: A taxonomy for autonomous agents. In *International workshop on agent theories, architectures, and languages* 21–35 (Springer, 1996).
- [28] Russell, S. & Norvig, P. Artificial intelligence. A modern approach 31–33 (Prentice Hall, Englewood Cliffs, 1995).
- [29] Huang, K. & Hughes, C. Introduction to agentic ai: Foundations, drivers, and risks. *Securing AI Agents: Foundations, Frameworks, and Real-World Deployment* 3–16 (Springer, 2025).
- [30] Yao, S. et al. React: Synergizing reasoning and acting in language models. In *The eleventh international conference on learning representations* (ICLR, 2022).
- [31] Wu, Q. et al. Autogen: Enabling next-gen llm applications via multi-agent conversations. In *First Conference on Language Modeling* (2024).
- [32] Li, G., Hammoud, H., Itani, H., Khizbullin, D. & Ghanem, B. Camel: Communicative agents for “mind” exploration of large language model society. In *Advances in Neural Information Processing Systems*, Vol. 36 51991–52008 (NeurIPS, 2023).
- [33] Zhang, K. et al. A survey of reinforcement learning for large reasoning models. *arXiv preprint arXiv:2509.08827* (2025).
- [34] Wang, L. et al. A survey on large language model based autonomous agents. *Front Comput Sci*, **18**, 186345 (2024).
- [35] Li, X., Wang, S., Zeng, S., Wu, Y. & Yang, Y. A survey on llm-based multi-agent systems: workflow, infrastructure, and challenges. *Vicinagearth*, **1**, 9 (2024).
- [36] Zhao, B. et al. Llm-based agentic reasoning frameworks: A survey from methods to scenarios. *arXiv preprint arXiv:2508.17692* (2025).
- [37] Tran, K. T. et al. Multi-agent collaboration mechanisms: A survey of llms. *arXiv preprint arXiv:2501.06322* (2025).
- [38] Rasal, S. & Hauer, E. Navigating complexity: Orchestrated problem solving with multi-agent llms. *arXiv preprint arXiv:2402.16713* (2024).
- [39] Du, Z. et al. Multi-agent collaboration via cross-team orchestration. In *Findings of the Association for Computational Linguistics: ACL 2025* 10386–10406 (ACL, 2025).
- [40] Dang, Y. et al. Multi-agent collaboration via evolving orchestration. *arXiv preprint arXiv:2505.19591* (2025).
- [41] Zhang, J., Fan, Y., Cai, K., Sun, X. & Wang, K. Osc: Cognitive orchestration through dynamic knowledge alignment in multi-agent llm collaboration. *arXiv preprint arXiv:2509.04876* (2025).

- [42] LangChain AI. Langgraph. <https://github.com/langchain-ai/langgraph> (2024).
- [43] Liu, J. Llamaindex. https://github.com/run-llama/llama_index (2022).
- [44] Radford, A. et al. Robust speech recognition via large-scale weak supervision. In *Proceedings of the 40th International Conference on Machine Learning*, Vol. 202 28492–28518 (PMLR, 2023).
- [45] Ravanelli, M. et al. Speechbrain: A general-purpose speech toolkit. *arXiv preprint arXiv:2106.04624* (2021).
- [46] Abouelenin, A. et al. Phi-4-mini technical report: Compact yet powerful multimodal language models via mixture-of-loras. *arXiv preprint arXiv:2503.01743* (2025).

10 Tables

Table 1 Example of SAOP workflow stage outcomes for each command

Agent	Command	Structure	Type	Expression	STT	CC	CR	AF	AP	AD	OF	IC
IR	Show patient information	Single	Explicit	Baseline	1	1	1	1	1	1	1	0
IR	Display the PFT info	Single	Explicit	Abbreviation	1	1	1	1	1	1	1	0
IR	Can you show pulmonary function test?	Single	NLQ	Baseline	1	1	1	1	1	1	1	0
IR	PFT results	Single	Implicit	Abbreviation	1	1	1	1	1	1	1	0
IR	lung function results	Single	Implicit	Paraphrase	0	1	1	1	1	1	1	0
IR	Show physical and PFT info	Composite	Explicit	Abbreviation	1	1	1	1	1	1	1	0
IR	Reset	Single	Implicit	Baseline	1	1	1	1	1	1	1	0
IV	Show the CT views	Single	Explicit	Baseline	0	1	1	1	1	1	1	0
IV	Coronal plus 100	Single	Explicit	Baseline	0	1	1	1	1	1	1	0
IV	Sagittal minus 30	Single	Explicit	Baseline	1	1	1	1	1	1	1	0
IV	Can you move CT forward?	Single	NLQ	Baseline	1	1	1	1	1	1	1	0
IV	Move front, front, front	Single	Implicit	Paraphrase	0	1	1	1	1	1	1	0
IV	Step to posterior	Single	Implicit	Paraphrase	0	1	1	1	1	1	1	0
IV	Axial zoom in	Single	Explicit	Baseline	1	1	1	1	1	1	1	0
IV	Can you get axial closer?	Single	NLQ	Paraphrase	1	1	1	1	1	1	1	0
IV	Minimize the axial image	Single	Explicit	Paraphrase	1	1	1	1	1	1	1	0
IV	Could you reduce coronal image?	Single	NLQ	Paraphrase	0	1	1	0	0	0	1	0
IV	Zoom out	Single	Implicit	Baseline	1	1	1	1	1	1	1	0
IV	Move axial to the middle slice and zoom in	Composite	Explicit	Paraphrase	1	1	1	1	1	1	1	0
IV	Can you move axial to 200 and coronal to 230?	Composite	NLQ	Baseline	0	1	1	1	1	1	1	0
AR	Show the 3D recon image	Single	Explicit	Baseline	1	1	1	1	1	1	1	0
AR	Can you load anatomical reconstruction?	Single	NLQ	Paraphrase	1	1	1	1	1	1	1	1
AR	Turn on RLL	Single	Explicit	Abbreviation	1	1	1	1	1	1	1	0
AR	Can you hide left lung?	Single	NLQ	Paraphrase	1	1	1	1	1	1	1	0
AR	Show anterior view	Single	Explicit	Baseline	1	1	1	1	1	1	1	0
AR	Can you look from the front?	Single	NLQ	Paraphrase	1	1	1	1	1	1	1	0
AR	Surgical view	Single	Implicit	Baseline	1	1	1	1	1	1	1	0
AR	Surgeon's view	Single	Implicit	Paraphrase	1	1	1	1	1	1	1	0
AR	Rotate to the right	Single	Explicit	Baseline	1	1	1	1	1	1	1	0
AR	Would you rotate up?	Single	NLQ	Baseline	1	1	1	1	1	1	1	0
AR	Can you zoom in to RLL?	Single	NLQ	Abbreviation	1	1	1	0	1	0	1	0
AR	Zoom out	Single	Implicit	Baseline	1	1	1	1	0	0	1	0
AR	Can you zoom in and rotate to the left?	Composite	NLQ	Baseline	1	1	1	1	1	1	1	0
AR	Can you initialize and zoom in?	Composite	NLQ	Baseline	1	1	1	1	1	1	1	0
AR	Can you erase all?	Single	NLQ	Paraphrase	1	1	1	1	1	1	1	0

STT: Speech-to-Text, CC: Command Correction, CR: Command Reasoning, AF: Agent Function, AP: Agent Parameters, AD: Action Determination, OF: Orchestration Flow, IC: Invalid Cycle, NLQ: Natural Language Question, IR: Information Retrieval, IV: Image Viewer, AR: Anatomy Rendering